Saharan dust contribution to PM10, PM2.5 and PM1 in urban and suburban areas of Rome: a comparison between single-particle SEM-

Journal of Environmental Monitoring

Dynamic Article Links

Cite this: *J. Environ. Monit.*, 2011, **13**, 732

www.rsc.org/jem

PAPER

Saharan dust contribution to PM_{10}, $PM_{2.5}$ and PM_1 in urban and suburban areas of Rome: a comparison between single-particle SEM-EDS analysis and whole-sample PIXE analysis†

Luca Matassoni,*[ab] Giovanni Pratesi,[ac] Damiano Centioli,[d] Fabio Cadoni,[d] Franco Lucarelli,[e] Silvia Nava[f] and Piergiorgio Malesani[acg]

Received 6th October 2010, Accepted 6th January 2011
DOI: 10.1039/c0em00535e

From February 15th to April 15th 2009, a period characterised by two episodes of Saharan dust outbreaks in Italy, particulate matter (PM) samples were collected at two stations (urban and suburban) in Rome. Some samples were selected and analysed using the SEM-EDS technique to characterise PM, focussing especially on the mineral contribution. Samples were representative both of days affected by Saharan dust episodes and days without this contribution. Cluster analysis allowed the attribution of each of about 67 000 analysed particles to one of the seven main statistical groups based on their composition. Characteristics of the particulate components identified using SEM-EDS analysis were verified by PIXE analysis carried out on filters collected in a suburban area. Ultimately, the contribution of crustal particles was revealed to be consistently high, highlighting the importance of local and regional mineral contributions, as well as those of Saharan origin. Therefore, quantifying all mineral contributions to resuspended particulate could lead to significant reductions of the PM level also on days not influenced by Saharan dust, thus limiting conditions when PM_{10} daily limit value (DLV) established by European legislation is exceeded.

[a]*Dipartimento di Scienze della Terra, Università di Firenze, Via La Pira 4, 50121 Firenze, Italy*
[b]*Prato Ricerche, Via Galcianese 20/H, 59100 Prato, Italy. E-mail: l.matassoni@pratoricerche.it; Fax: +39 0574 447725; Tel: +39 0574 447722*
[c]*CESPRO, Università di Firenze, Viale Morgagni 48, 50134 Firenze, Italy*
[d]*ISPRA, Istituto Superiore per la Protezione e la Ricerca Ambientale, Via di Castel Romano 100, 00128 Rome, Italy*
[e]*Dipartimento di Fisica e Scienze dello Spazio, Università degli Studi di Firenze, Via Sansone 1, 50019 Sesto Fiorentino, Italy*
[f]*INFN, Istituto Nazionale di Fisica Nucleare, Sezione di Firenze, Via Sansone 1, 50019 Sesto Fiorentino, Italy*
[g]*CABeC, Università di Firenze, Via La Pira 4, 50121 Firenze, Italy*
† Electronic supplementary information (ESI) available: Fig. S1–S13 and Table S1. See DOI: 10.1039/c0em00535e

1. Introduction

Several studies[1,2] have shown the impact of the mineral component of atmospheric particulate matter (PM) on the environment and human health. However, European legislation provides that the contributions recognised as natural sources, including natural particles transported from dry regions, can be subtracted from the total PM_{10} value measured by the air quality monitoring networks of member states (EU Directive 2008/50/EC).

Previous studies have shown that the potential for Saharan dust episodes in Europe and the Mediterranean area is high.[3–7] These episodes may cause exceedances of the PM_{10} daily limit value (DLV of 50 μg m^{-3}).

Environmental impact

PM concentration values measured in Italy can be influenced by the advection of Saharan dust that can also cause exceedances of the PM_{10} daily limit value established by European Union. Focussing the attention on the mineral contribution to PM, the study showed that comparison between single-particle and whole-sample analysis can help to distinguish the different sources. The authors highlighted the complex composition of many particles. Moreover, PM composition showed some differences during the days affected by Saharan dust compared to those without such inflow. A local crustal contribution to PM in Rome was inferred by the variation of the Si/Al ratio values, probably also due to re-suspended particles. A correct evaluation of this contribution represents a primary goal for politicians because this could lead to reduce PM_{10} DLV exceedances, in spite of negative impact on human health also due to this re-suspended dusts.

Based on a multi-year dataset representative of background stations in Italy, Matassoni *et al.*[6] found a decreasing influence of Saharan dust on PM_{10} DLV exceedances from south to north (from 97% in Sicily to 40% in Lazio to 8% in Emilia–Romagna region), mainly due to the larger distance from the dust sources.

This study aims to identify the various contributions to PM, with particular attention to the crustal mineral component, in an intermediate location in central Italy, Rome (Lazio). At the same time, the study highlights differences in the composition of individual particles between days affected by Saharan dust, here called "in-dust days," and those without such inflow, here called "non-dust days."

2. Methodology

2.1. Sampling methods

The particulate matter was collected at two stations in the Rome area 27 km apart from each other (Fig. 1), defined as "urban traffic" and "suburban background" according to the criteria for Euroairnet:[8,9]

Corso Francia (CF): located in the northern urban area at a main cross roads affected by high traffic volume (41.70° N, 12.45° E) and belonging to the monitoring network station of the Regional Environmental Protection Agency (ARPA Lazio); here PM_{10} and $PM_{2.5}$ samples were collected and concentration values measured.

Castel Romano (CR): located in the southern suburban area, about 500 m from a main road affected by high traffic volume (41.95° N, 12.47° E) and near the car parking area of the Istituto Superiore per la Protezione e la Ricerca Ambientale (ISPRA), which provided the equipment for the collection of the PM_{10}, $PM_{2.5}$ and PM_1 samples and for the measurement of the relative concentration values.

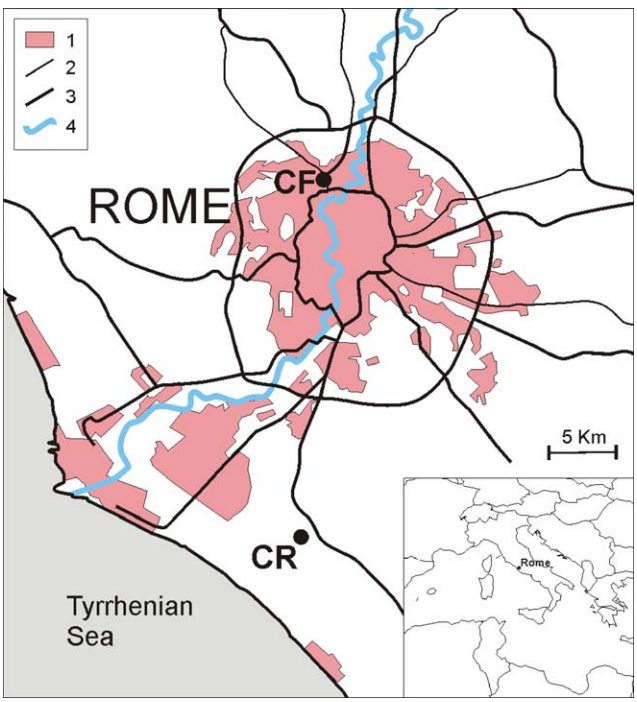

Fig. 1 Localisation of the Corso Francia (CF) and the Castel Romano PM stations. Legend: 1, urban areas; 2 and 3, main roads; 4, Tevere river.

To obtain an accurate sampling of the particulate matter, we used the following equipment, in compliance with European (EN12341, EN14907) and/or US (EPA40CFR) standards: Tecora Charlie and Skypost PM (PM_{10} and $PM_{2.5}$) Thermo Partisol Plus 2025 (PM_1).

The PM_{10} and $PM_{2.5}$ daily concentration values at the CF station were provided by ARPA Lazio using the Fai SWAM 5A β-ray attenuation monitor and at the CR station were recorded by Thermo TEOM 1400A equipped with an FDMS C tool kit.

Key meteorological parameters, such as temperature, pressure, rainfall, humidity, wind speed and direction, were acquired at the CR station. In addition, weather parameters were complemented with NOAA Earth System Research Laboratory charts (available at http://www.cdc.noaa.gov/Composites/day/).

Preliminary tests and previous studies[10–12] led us to select polycarbonate filters (Millipore) with a diameter of 47 mm and 0.8 μm pores and to determine optimum flows for sampling under different conditions. The sampling time ranged from 8 to 60 minutes per hour over 24 hours total to avoid excessive overlapping of particles on the filter, even in the case of daily concentrations above 50 μg m^{-3}.

The sampling period for PM analysis, February 15th to April 15th 2009, was selected according to a previous experiment[6] and the TAU model Desert Dust Forecast of the Weather Research Centre of Tel-Aviv University (images available at http://wind.tau.ac.il/dust8/dust.html).[13]

Within this period, 9 in-dust-day samples complemented by another 21 non-dust-day samples (30 days of samples overall) were selected.

2.2. Operating procedure of the SEM-EDS analysis

The analysis of individual particles was carried with a Scanning Electron Microscope (Zeiss EVO MA15) equipped with an Oxford Inca 250 energy dispersive detector.

The system employs the Inca Suite software (version 4.13, Oxford Instruments, UK) for elemental and morphometric sample analysis, which is controlled by a computer after the initial instrumental conditions are set.

The portions of each of the 150 selected filters (five samples—relating to three PM fractions at CR and two PM fractions at CF—for each of the 30 days considered) were mounted on aluminium stubs (12.5 mm diameter) and metallised with carbon.

The thresholds for the recognition of individual particles were chosen by taking blank portions of filter as references and comparing them to backscattered electron (BSE) images with secondary electron (SE) ones,[10,14] so as to allow detection of the maximum number of particles while avoiding the recognition of false particles. This procedure prevented the correct identification of the carbonaceous, organic and biological particles, which were not the objective of the study. In any case, careful choice of thresholds allowed the recognition of sulfate particles even in the finer fractions.

We set minimum size thresholds for the recognition of particles in PM_{10} and $PM_{2.5}$ fractions to ensure that a significant number of particles of various sizes were analysed. Assuming a characteristic density of 2.7 g cm^{-3} for crustal particles, particles with

ECD (Equivalent Circle Diameter) less than 1.5 μm (corresponding to an aerodynamic diameter of 2.5 μm) were excluded from the analysis of PM_{10} samples, whereas particles with ECD less than 0.6 μm (corresponding to an aerodynamic diameter of 1 μm) were excluded in the analysis of $PM_{2.5}$. However, the detection limit of particles in the PM_1 samples was determined by the smallest feature width.

The acquisition time of the X-radiation produced by samples was set at 8 s for particles containing silicon and at 4 s for the other particles. The X-ray spectrum acquired for each detected particle was processed through the XPP[15] correction procedure implemented in the Inca software package (Oxford Instruments, UK).

2.3. SEM-EDS data acquisition and pre-treatment

The analyses were performed using the following operating conditions: working distance 9 mm, acceleration voltage 20 kV and beam current 0.1 nA. These settings allowed for the detection of between 400 and 1000 particles (20–40 particles per field of view), which ensured the representativeness of the entire filter.[10] The setting of the numbers of particles for detection allowed for the recognition of at least 10 fields for each analysed sample. Each analysis session always started with an initial beam calibration process through a sample of cobalt.

The following data were acquired with the aim of achieving complete information on the PM:

- spectra and total counts of X-rays, from which is obtained the composition of individual particles as a percentage by weight of the elements (wt%);

- morphological characteristics of each particle, such as area (A), length (largest Féret's diameter), width (smallest Féret's diameter), aspect ratio (the ratio of the minimal to the maximal Féret's diameter), perimeter (p) and the ECD ($[4A/p]^{½}$);

- BSE images of fields and particles analysed.

A selection of SE images was also manually obtained. These data were then stored in electronic format for subsequent processing.

Only elements with a significant number of particles (at least 1% in one or more of the various fractions of PM) were considered during data analysis and interpretation, excluding C and O because they are components of the filter.

Ultimately, we selected the following elements for this study: Na, Mg, Al, Si, P, S, Cl, K, Ca, Ti, Mn, Cr, Fe, Cu, Zn, Mo, Br, Ba and Pb.

The data were then grouped by dividing Saharan dust-affected days (in-dust) from those without this contribution (non-dust).

About 6.5% (1% in the PM_{10} samples, 9% in the $PM_{2.5}$ samples and 14% in the PM_1 samples) of over 71 000 particles analysed were excluded from further processing; these particles were mainly composed of C and O or, much less frequently, by other underrepresented elements.

2.4. PIXE analysis of the Castel Romano samples

PIXE analysis (Particle-Induced X-ray Emission) was performed on all of the particulate fractions sampled in the suburban area (CR) to complete the study and to obtain information on mass concentration of elements. Samples collected in the urban area (CF) were not analysed by PIXE due to the very low particulate load collected on these filters: indeed, the sampling flow at CF was set at the lowest level to allow the detection of single particles by SEM.

The PIXE analyses were carried out at the 3 MV Tandetron accelerator of the LABEC laboratory (National Institute of Nuclear Physics, Sezione di Firenze), where a beam line is fully dedicated to the analysis of atmospheric aerosol and specific procedures have been developed for the analysis of different kinds of aerosol samples.[16] These analyses were performed by bombarding filters with a 3.06 MeV protons beam, collimated to a rectangular spot (1×2 mm^2). Acquisition times for each sample were 60 s for PM_{10}, 300 s for $PM_{2.5}$ and 400 s for PM_1. During irradiation, the filter was moved in front of the beam so that most of the area of deposit was sampled. Elements from Na to Ca were measured using an SDD (Silicon Drift Detector), while other elements with higher atomic numbers were measured using an Si(Li) detector. The instrumental set-up is reported in Chiari *et al.*[17] and Calzolai *et al.*[18]

The PIXE spectra were analysed using the GUPIX software package.[19] Having information on the sampling parameters such as area of storage, air flow rate and duration of sampling, the elemental concentrations were obtained using a calibration curve based on a set of Micromatter thin standards with a known areal density. The detection limits were about 10 ng m^{-3} for elements with low atomic numbers and about 1–2 ng m^{-3} for elements with medium to high atomic numbers. The elements detected in the samples were as follows: Na, Mg, Al, Si, S, Cl, K, Ca, Ti, V, Cr, Mn, Fe, Ni, Cu, Zn, Br, Sr and Pb. In addition to the elements measured in the SEM-EDS, V, Cr, Ni and Sr were also analysed; however, P, Mo and Ba were not analysed by PIXE.

3. Results and discussion

3.1. Identification and assessment of Saharan dust inputs

Movements of the air masses in the period between February 15th and April 15th 2009 were investigated with the aim of establishing the origin of the particulate matter collected on the filters and distinguishing the in-dust days from non-dust days. According to Matassoni *et al.*,[6] the back-trajectories were computed using the HYSPLIT (HYbrid Single-Particle Lagrangian Integrated Trajectory) model and results were integrated and validated using other available data.

Following the procedure mentioned above, two main Saharan dust input periods were revealed, namely from March 1st to March 4th (Fig. S1†) and from March 28th to April 1st (Fig. S2†), amounting to 9 in-dust days during the study period. In addition to the samples related to the Saharan dust episodes, other samples representative of 21 non-dust days were selected to be investigated with SEM and analysed with EDS.

The analysis of the synoptic conditions revealed a system of "low-high" cells that was characteristic of the in-dust days and differs both from the 1968–1996 climatology as well as from the mean of the sampling period (Fig. S3†). Such reconstruction confirms the meaningful meteorological differences occurring between in-dust and non-dust days,[6] and accounts for a comparative analysis of the related data allowing the

identification of peculiar features in the distribution of the single particles.

The mean values of the PM_{10} and $PM_{2.5}$ concentrations, measured at CR and CF and associated with the days chosen for the study, are listed in Table S1†. Six days with PM_{10} DLV exceedance (three of them occurring during in-dust events) were identified at the CF station, whereas no exceedances were revealed at CR confirming the suburban typology of this station. The exceedances occurring during the non-dust days were mainly due to anthropogenic causes, above all traffic pollution.[6] Moreover, it is noteworthy that wind and rain effectively contributed to decreasing the daily concentration of PM_{10} (Table S1†).

According to the methodology suggested by Escudero *et al.*,[4] already employed in a similar context,[6,7] the Saharan contribution to the PM_{10} concentration at the CF station has been quantified. The differences between PM_{10} values of in-dust days and the monthly moving 30th percentile calculated for non-dust days on the same dates account for two of the three DLV exceedances that occurred in the urban area during the in-dust days (Fig. S4†). Only the exceedance that occurred on March 30th remains, since the PM_{10} concentration only dropped to 58 $\mu g\ m^{-3}$ after the subtraction of the background value (corresponding to 20 $\mu g\ m^{-3}$) calculated for the CR station on the same day.

3.2. Cluster analysis of SEM data

Preliminarily, the particles composed of only one among the selected elements (hereafter referred to as "mono-elemental") amounted to 10% of particles on in-dust days and 19% on non-dust days.

Among these mono-elemental particles included those composed of Fe, and, in decreasing order, S, Si, Na and Ca in the PM_{10} and $PM_{2.5}$ fractions; conversely, the PM_1 fraction included particles clearly composed of S, followed by those composed of Fe, Si (particularly during in-dust days), Na and Ca (Fig. S5†).

The elemental composition of the other 55 400 particles was statistically analysed using the MYSTAT software package, ver. 12 (Systat Software, Inc., Chicago, IL), with the aim of distinguishing the sources of the different fractions of particulate.

A search for homogeneous particle clusters was performed through a cluster analysis using the non-hierarchical *k*-means method. This technique is often employed in PM investigations,[20,21] in this case measured the dissimilarity between objects by Euclidean distance.

The analysis was performed by testing several solutions with a cluster number from five to twelve for all of the ten groups of data (three fractions at CR and two fractions at CF, both for in-dust and non-dust days) and by selecting the initial seed points on the basis of the Principal Component Analysis results. The optimal solution, obtained in such a way as to make the resulting clusters comparable to each other in the different PM fractions and typologies, subdivides all analysed data into seven clusters. One of the clusters is referred to as VMC (Variable Mixing Cluster), indicating that its elemental composition is not well defined compared to the other clusters.

Table 1 provides the mean of the major elements characterising the seven clusters, named according to the prevailing elements. The percentage distribution of the examined single particles is shown in Fig. 2 where data have been arranged to show frequency of observations within the clusters both for PM size and Saharan dust outbreaks.

Some binary and ternary plots have been generated to gain better knowledge of the different PM sources and to verify the fitness of the chosen clusters. These plots show the polyphasicity of many particles and moreover suggest a possible interpretation of such features. To make the diagram interpretation straightforward, only the particles that were really composed of all considered elements have been taken into account, whereas those lying on the axes have been excluded.

3.2.1. Crustal contribution to PM. The percentage distribution of the [Si, Al] cluster in several fractions clearly showed its prevalence during the in-dust days (over 50% at CR station), which ascribes a prevailing Saharan origin to the particles within this cluster. A similar consideration can be argued about the [Si] cluster, although its increase during the dust-affected days was very slight. In any case, the persistence of the two above-mentioned clusters during the days that were lacking in Saharan dust outbreaks suggests a crustal contribution yielded by resuspension of dust coming from proximal (regional) areas as well as of materials previously carried from distal sources. However, contribution of traffic and in smaller amount of industrial sources cannot be excluded.

The particles that comprise Saharan dust are created by a natural sandblasting process that removes small particles originating from surface fracturing of larger particles.[22–24] These small particles are composed mainly of mineral aggregates, but they can also be monophasic (in particular quartz and "clay" minerals). The [Si–Al] binary graphs (Fig. 3) represent this concept well, showing that the dots of the cluster are in greater numbers in the central area. As a comparison, the compositions of some pure silicates have been reported in the graphs.

In the zone of transition toward the [VMC] cluster, owing to the increase of other elements, there is a trend of contemporaneous decrease in the Si and Al content of the particles. Another ideal line links the centre of the [Si, Al] cluster area with the 100% corner on the Si axis, therefore suggesting a trend characterised by an increase in Si and the simultaneous decrease in Al as long as the composition of pure quartz has been attained.

As a matter of fact, the Si–Al diagrams do not show strong differences in the composition of PM, either between in-dust and non-dust days or between urban and suburban areas. In any case the [Si, Al] and [Si] clusters are more compact during in-dust days (smaller extension of the confidence ellipse at 95%; *cf.* Fig. 3).

However, the Si/Al mass ratios are in the range of 1.5–3.9 (Fig. 3) and are therefore consistent with those evidenced in other papers and connected with the aggregation of several clay minerals along with quartz.[21,25]

The mean composition of the [Si, Al] and [Si] clusters suggests that the more representative elements in the particles are Fe, Ca and S, other than those characterising the cluster itself. The particles containing Fe and Ca could be mainly related to proximal (local or regional) sources, as the particular soil composition of the Roman Magmatic Province can account for them (see the following paragraph). Conversely, the S content is associated with the covering of many [Si, Al] and [Si] cluster particles by sulfates;[25,26] in addition, such a covering may also occur in particles from other clusters.

Table 1 Weight percent average and standard deviation of the main elements characterizing clusters identified, non-dust days (above) and in-dust days (below)

	CR			CF	
Cluster	PM_{10}	$PM_{2.5}$	PM_1	PM_{10}	$PM_{2.5}$
Non-dust days					
[Si, Al]	Si (44.3 ± 10.7) Al (17.5 ± 7.1) Fe (8.2 ± 7.1)	Si (48.8 ± 10.1) Al (19.3 ± 7.6) Fe (8.7 ± 8.4)	Si (57.2 ± 14.6) Al (16.0 ± 9.9) Fe (7.0 ± 9.3)	Si (50.9 ± 6.9) Al (18.5 ± 4.9) K (11.2 ± 10.3)	Si (49.9 ± 7.2) Al (18.3 ± 6.9) Fe (8.4 ± 8.1)
[Fe]	Fe (76.4 ± 17.1) Na (4.5 ± 7.6)	Fe (78.9 ± 15.9) S (7.5 ± 8.7)	Fe (70.3 ± 15.1) S (12.2 ± 12.7)	Fe (81.1 ± 17.5) Si (4.3 ± 4.4)	Fe (78.9 ± 20.1) Na (5.2 ± 8.8)
[VMC][a]	Ca (36.8 ± 30.5) Si (17.5 ± 15.1) Na (15.1 ± 21.3) Cl (8.2 ± 12.5)	Si (25.5 ± 15.0) Ca (20.7 ± 13.2) S (13.7 ± 11.9) Al (7.1 ± 6.9)	S (16.1 ± 17.0) Si (15.5 ± 18.1) Zn (11.1 ± 23.8) Cu (8.9 ± 22.5)	Ca (31.7 ± 26.6) Si (27.7 ± 13.7) Fe (8.6 ± 8.5) Al (8.1 ± 5.5)	Al (16.4 ± 14.5) K (14.9 ± 21.8) Ca (14.6 ± 22.0) Si (13.3 ± 16.1)
[S]	S (38.6 ± 7.1) Na (34.4 ± 10.1) Ca (14.6 ± 9.2)	S (42.1 ± 24.4) Na (20.1 ± 24.6) K (8.0 ± 12.5)	S (53.4 ± 14.2) Na (27.7 ± 19.0) K (11.8 ± 16.1)	—	Na (44.3 ± 12.3) S (43.2 ± 10.6) Ca (6.5 ± 10.4)
[Si]	Si (82.3 ± 10.4) Al (4.3 ± 4.5)	Si (79.8 ± 8.0) Al (5.8 ± 6.9)	—	Si (85.6 ± 9.9) Al (4.1 ± 4.8)	Si (73.4 ± 10.3) Al (14.6 ± 10.2)
[Ca, S]	Ca (44.3 ± 10.1) S (36.0 ± 8.0)	Ca (62.1 ± 15.8) S (21.3 ± 17.5)	Ca (53.9 ± 16.4) S (27.3 ± 19.2)	Ca (43.0 ± 13.7) S (37.9 ± 8.7) Na (8.7 ± 10.7)	Ca (46.7 ± 11.3) S (38.5 ± 6.7) Na (6.8 ± 8.7)
[Cl, Na]	Cl (57.8 ± 5.6) Na (37.0 ± 4.3)	Cl (60.0 ± 7.0) Na (35.7 ± 6.8)	—	Cl (48.8 ± 13.1) Na (35.4 ± 10.3)	Cl (57.2 ± 9.7) Na (37.0 ± 7.2)
In-dust days					
[Si, Al]	Si (44.3 ± 8.5) Al (17.6 ± 5.9) Fe (9.5 ± 6.1)	Si (49.6 ± 8.4) Al (19.2 ± 5.0) Fe (9.5 ± 5.8)	Si (51.7 ± 7.5) Al (20.1 ± 6.4) Fe (9.3 ± 7.9	Si (51.0 ± 7.3) Al (19.0 ± 5.8) Fe (9.0 ± 5.2)	Si (51.1 ± 9.6) Al (19.5 ± 6.6) Fe (10.5 ± 8.6)
[Fe]	Fe (72.3 ± 16.7) Si (6.8 ± 6.8)	Fe (77.7 ± 12.0) Na (5.0 ± 7.8)	Fe (60.3 ± 15.4) S (8.4 ± 8.3)	Fe (86.0 ± 8.3) Si (4.7 ± 3.2)	Fe (84.4 ± 9.7) Na (4.2 ± 8.4)
[VMC][a]	Si (19.8 ± 9.5) Na (15.1 ± 10.5) S (13.9 ± 11.0) Ca (12.9 ± 10.4)	Si (30.9 ± 10.0) S (15.7 ± 10.4) Al (11.3 ± 7.4) Fe (10.5 ± 12.9)	Si (18.5 ± 18.5) S (17.7 ± 15.0) K (12.8 ± 17.0) Na (7.2 ± 9.9)	Ca (25.9 ± 23.8) Si (21.0 ± 13.2) Fe (13.0 ± 17.0) Al (7.6 ± 8.2)	Si (28.8 ± 17.0) S (17.5 ± 12.8) Ca (11.7 ± 13.8) Fe (11.3 ± 17.5)
[S]	S (51.3 ± 12.6) Na (22.1 ± 16.5) K (18.3 ± 11.9)	S (41.2 ± 11.8) K (33.4 ± 17.6) Na (15.6 ± 13.9)	S (57.0 ± 9.7) K (26.9 ± 14.4) Na (15.7 ± 15.4)	—	S (44.0 ± 8.9) Na (40.6 ± 17.4) K (12.0 ± 18.4)
[Si]	Si (78.2 ± 10.1) Al (5.4 ± 4.1)	Si (78.4 ± 8.8) Al (6.2 ± 5.4)	Si (75.4 ± 9.2) Al (6.6 ± 7.9)	Si (83.3 ± 9.1) Al (6.1 ± 5.5)	Si (81.9 ± 8.4) Al (8.1 ± 8.0)
[Ca, S]	Ca (42.7 ± 11.6) S (36.8 ± 12.7)	Ca (41.6 ± 14.0) S (35.5 ± 11.4)	Ca (49.1 ± 13.4) S (34.9 ± 20.0)	Ca (53.6 ± 4.7) S (41.5 ± 3.7)	Ca (50.7 ± 10.7) S (40.9 ± 10.2)
[Cl, Na]	—	—	—	—	—

[a] VMC as variable mixing cluster.

3.2.2. Other mineral contributions. The Fe-rich particles found in PM can be related to two different sources: on the one hand, there is the natural influence of crustal contributions to PM; on the other hand, there is the contribution of anthropic sources.[27]

According to the analyses performed by the authors, the [Fe] cluster, widespread in all of the three PM fractions without any difference between CR and CF stations, seems to be more important than previously reported in the literature. Nevertheless, its percentage of incidence was higher during non-dust days (even over 40%), mainly in the urban environment where the CF station was located (Fig. 2).

This result suggests a proximal (local or regional) origin of at least a portion of the [Fe] cluster particles, probably due to the widespread presence of Fe in the soil of the Lazio (FeO topsoil map at http://www.gtk.fi/publ/foregsatlas/)[28] and, in particular, of the Roman area, where volcanites (rich in femic minerals such as pyroxenes and spinels) outcrop, slightly north of the urban area and not far from the CF station; however, an anthropic contribution due to the traffic cannot be excluded. It is worth mentioning that, even in this cluster, a polyphasic composition of many particles occurs.

In the [VMC] cluster, many particles are still affected by a [Si, Al] composition, but with greater amounts of other elements such that a femic nature can be argued for some of these particles. In any case, it is quite clear that the particles belonging to the [VMC] cluster represent transition terms among the elements of other clusters. Finally, then, this cluster cannot only be related to one source.

With regard to the PM_{10} and $PM_{2.5}$ fractions, it is noteworthy that a Ca component prevails, especially during non-dust days and in the urban environment (ideal tendency line towards 100% of Ca, as can be seen in Fig. S6†).

During in-dust days, such a component was less evident in the urban environment (CF station) and did not appear at all in the suburban environment (CR station), making a proximal source probable. This source may be connected with the outcropping of Ca-rich soils that occurs in the Lazio and, in particular, in the Roman area where, as previously reported about the [Fe] cluster, there is an occurrence of volcanic rocks not far from the CF

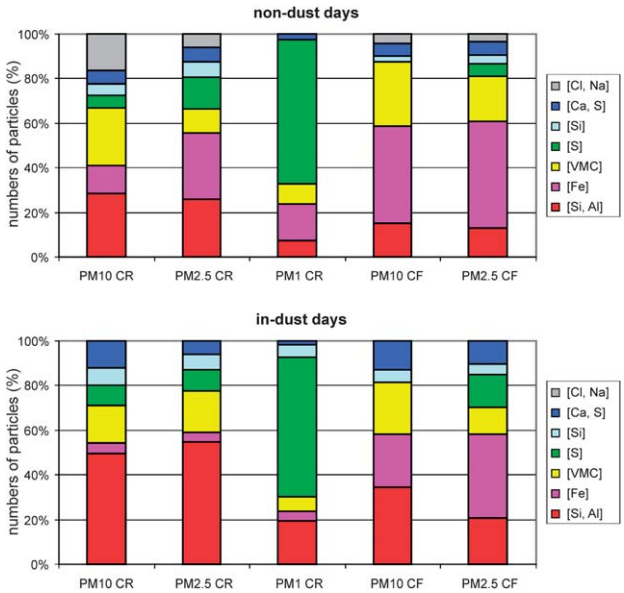

Fig. 2 Particle number (percent) of the different clusters identified in each fraction of PM at the two locations (CF and CR): non-dust days (above) and in-dust days (below). Figures included mono-elemental particles, attributing to the different clusters.

station (CaO topsoil map at http://www.gtk.fi/publ/foregsatlas/).[28]

3.2.3. Anthropic contribution. S-rich particles are usually recognised as a marker of anthropic influence, mainly when they occur in the finer fractions. Therefore, the [S] cluster assumed great importance only in the PM_1 fraction (Fig. 2), where it was absolutely dominant (incidence equal to or greater than 60%). As far as the $PM_{2.5}$ fraction is concerned, it was characterised by a greater sulfur amount, mainly in the urban environment, in comparison with the PM_{10} fraction, thus confirming its anthropogenic origin. Ternary plots relative to $PM_{2.5}$ (Fig. 4) show also closeness with the [Ca, S] cluster.

In Fig. 4, three trending lines, starting from the "Others" vertex, can be argued:[21] the first one, elongated towards the S + Cl + P composition and characterised by a low percentage of Ca, represents the aggregates of quartz–silicatic particles, along with salts of secondary origin such as $(NH_4, Na, K, Mg)_x(SO_4, PO_4, Cl)_y$; the second line, tending towards (Ca) composition, describes particles composed of quartz–silicatic aggregates along with $CaCO_3$; and the third line, tending towards the value 0.55 on the Ca axis, represents the theoretical point of $CaSO_4$ in the graphs.

These particles of impure $CaSO_4$ come mainly from the interaction of the pollutant SO_2 with the Ca-carbonatic mineral component.[2,29] Moreover, the reduced importance of the Ca component during the in-dust days was apparent, evidenced by the lack of a corresponding ideal tendency line.

Since Ca–S binary plots (Fig. S7†) display a better definition of the [Ca, S] cluster during in-dust days compared to non-dust days (smaller extension of the confidence ellipse at 95%), at least a few gypsum particles probably can be ascribed to Saharan dust outbreaks.[30]

Other elements characterising the [S] cluster are Na and K; Ca is also present because of the already described contiguity with

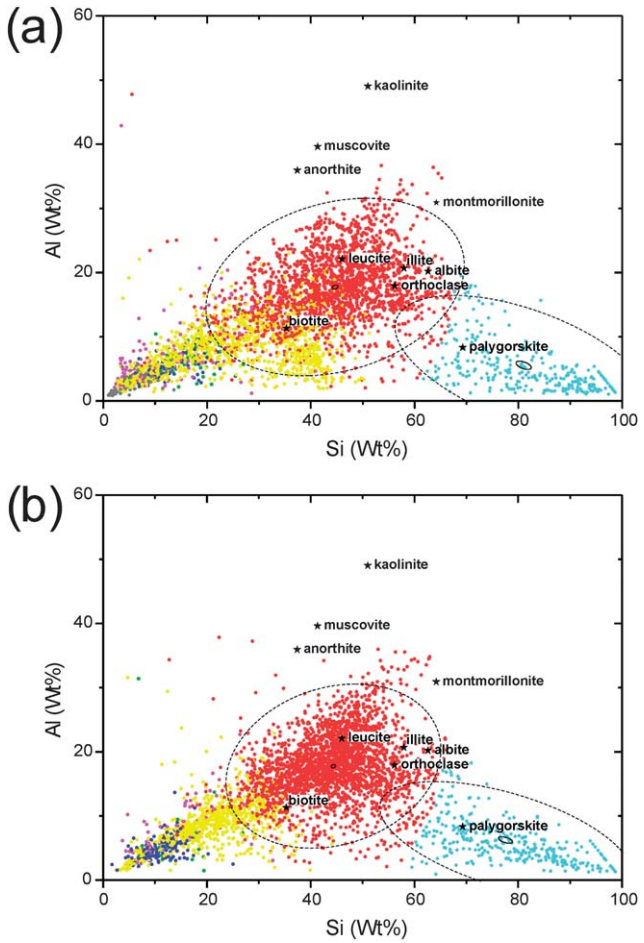

Fig. 3 Si–Al binary graphics for the PM_{10} at CR station, non-dust days (a) and in-dust days (b). Graphics showed compositions of some minerals and confidence ellipses of 95% (prediction and mean) for [Si, Al] and [Si] clusters. See color legend in Fig. 2.

the [Ca, S] cluster (Table 1). Occurrence of sodium sulfate particles can be related to a double factor: particles characterised by an almost unitary Na/S atomic ratio are conceived to be secondary pollutants, such as $NaHSO_4$ or CH_3SO_3Na; the excess of S or Na, along with the presence of other cations, may suggest that some particles result from aggregation of $CaSO_4$, NaCl and Na_2SO_4.[26] On the other hand, as previously outlined, sulfur tends to cover pre-existing solid particles; in fact, its widespread occurrence in many particles clearly demonstrates that secondary sulfates nucleate heterogeneously on primary solid particles.[25,26]

3.2.4. Sea contribution. The [Cl, Na] cluster, clearly related to marine aerosols, mainly occurred in the 2.5–10 μm fraction on non-dust days; by contrast, it totally disappeared during in-dust days (Fig. S8†), probably due to the behaviour of the hygroscopic NaCl particles that favour aggregation with silicate particles,[31] which are more abundant in the Saharan dust outbreaks. An alternative explanation could be connected to the dynamics of Saharan dust downfall—whose transport takes place at relatively high altitudes (1000–5000 m above sea level) without necessarily involving the lowermost layers—which may imply an atmospheric circulation limiting the proximal marine

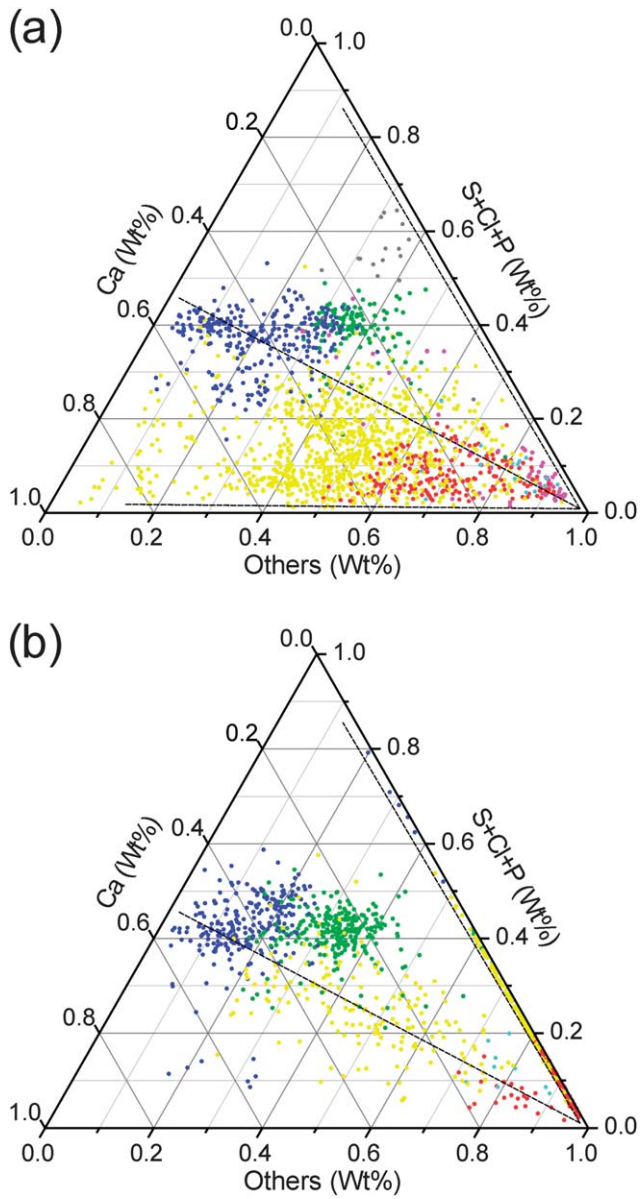

Fig. 4 Others–Ca–S + Cl + P ternary graphics for the $PM_{2.5}$ at CR, non-dust days (a) and in-dust days (b). Others is the sum of all the elements considered in the analysis do not appear in the other vertices. See color legend in Fig. 2.

contribution. The alignment of many particles with the ideal connection line from the origin of the diagram to pure end-member composition (halite) attests to a polyphasic composition, which accounts for the substantial attribution to the [VMC] cluster.

3.3. PM morphological analysis

Particle morphology was investigated using two parameters automatically obtained by SEM image analysis software: the diameter of the ideal circular (spherical) particle equivalent to that of the real particle (ECD) and the aspect ratio (*i.e.*, the ratio of the minimal to the maximal Féret's diameter).

Fig. S9†, summarising the percent distribution of the particles of the different clusters according to their size, reveals that [S] cluster particles prevailed, usually in the PM_1 fraction. Analogously, it has been established that the amount of [Si, Al] cluster particles decreases with a reduction in diameter size, therefore confirming that crustal particles dominate in PM_{10} whereas anthropic particles are more abundant in PM_1. With regard to the [VMC] cluster, its particles were more frequent in the coarser fraction probably due to the presence of Ca-rich particles.

It is worth noting that, during in-dust days, the [Si] and [Si, Al] clusters became more widespread even in the finer fractions ($PM_{2.5}$ and PM_1), indicating a significant contribution of Saharan dust to this fraction. Finally, the [Cl, Na] cluster was completely absent from the finest fraction.

The distribution of the particles into several size fractions points out a maximum with respect to diameters ranging from 1 to 2.5 μm and a small amount of particles with an equivalent diameter >5 μm. These features are mainly related to a couple of concomitant factors: dealing with the equivalent circular diameter, the maximum sizes of the particles are often underestimated; the crustal particles, sampled by an instrument that yields an aerodynamic "cut" at the nominal threshold of 10 μm, as a matter of fact looked to have a diameter centred at about 6 μm, considering a mean density of 2.7 g cm^{-3}.

The aspect ratio diagram (Fig. S10†) shows the strongest irregularity of the [S] cluster particles opposite to the uniformity of the [Cl, Na] cluster particles. Such a feature, also evidenced by the SE images displaying the prevalent elongated morphology of the sulfate particles and the more rounded morphology of the silicate and NaCl particles, is in agreement with the literature on this subject.[32]

3.4. PIXE results

Table 2 shows the elemental concentration values (mean values with standard deviation, minimum and maximum) for the various PM fractions.

The sum of the concentrations of all the elements detected by PIXE was generally much lower than the PM concentration measured by TEOM both for PM_{10} and $PM_{2.5}$ fractions (Fig. S11†). Note that PM_1 has not been measured.

The average particulate fraction determined by PIXE analysis was 18% for PM_{10} and 11% for $PM_{2.5}$, with higher percentages during Saharan episodes (in-dust days) due to the higher contribution of the soil component and lower percentages during the most polluted days when carbon compounds are predominant. The PM mass fraction which is not explained by PIXE is mainly composed of H, C, N and O, major aerosol elements that cannot be detected by this technique.

The average percentages by weight of the elements in the various fractions of PM, both for in-dust and non-dust days, were calculated to facilitate comparison with data from individual particle analysis (Fig. S12†).

As already stated on the basis of SEM-EDS analysis, data reduction proves the progressive predominance of S with decreasing size fraction of PM, the increased importance of Si and Al on in-days and that of Ca during non-dust days (at least for the PM_{10} fraction). However, the increased importance of Fe on non-dust days and in the $PM_{2.5}$ fraction compared to PM_{10},

Table 2 Concentration values of the elements (μg m^{-3}) by PIXE analysis, non-dust days (above) and in-dust days (below). Minimum error of 10% for min and max of 5% for mean and standard deviation

Non-dust		Na	Mg	Al	Si	S	Cl	K	Ca	Ti	V	Cr	Mn	Fe	Ni	Cu	Zn	Br	Sr	Pb
PM_{10}	Mean	0.98	0.21	0.32	0.81	1.36	0.70	0.46	0.89	0.024	0.011	0.009	0.010	0.47	0.004	0.021	0.033	0.011	0.006	0.011
	St. dev.	0.66	0.13	0.35	0.84	1.26	0.92	0.46	0.83	0.025	0.006	0.005	0.009	0.44	0.004	0.019	0.030	0.008	0.005	0.009
	Min	0.055	0.022	0.037	0.12	0.12	0.019	0.049	0.10	0.004	0.006	0.003	0.001	0.052	0.001	0.002	0.001	0.001	0.001	0.001
	Max	2.3	0.50	1.9	4.7	6.8	3.4	2.1	2.9	0.12	0.022	0.019	0.033	1.9	0.014	0.073	0.12	0.033	0.017	0.036
$PM_{2.5}$	Mean	0.144	0.038	0.029	0.072	0.45	0.103	0.105	0.031	0.006	0.003	0.002	0.001	0.031	0.002	0.003	0.008	0.003	0.001	0.005
	St. dev.	0.26	0.045	0.045	0.092	0.32	0.31	0.090	0.029	0.007	0.001	0.001	0.001	0.027	0.001	0.003	0.005	0.002	0.001	0.010
	Min	0.017	0.008	0.007	0.022	0.027	0.010	0.016	0.007	0.001	0.001	0.001	0.001	0.002	<0.001	<0.001	0.001	0.001	0.001	<0.001
	Max	1.2	0.20	0.26	0.61	1.4	1.6	0.60	0.17	0.017	0.005	0.007	0.003	0.16	0.007	0.015	0.031	0.011	0.002	0.066
PM_1	Mean	0.035	0.011	0.019	0.050	0.45	0.014	0.110	0.009	0.002	0.002	0.001	0.001	0.011	0.001	0.001	0.006	0.004	<0.001	0.002
	St. dev.	0.019	0.003	0.012	0.032	0.18	0.007	0.076	0.005	<0.001	0.001	<0.001	<0.001	0.007	<0.001	0.001	0.003	0.001		0.001
	Min	0.008	0.007	0.007	0.025	0.19	0.006	0.027	0.004	0.002	0.002	0.001	0.001	0.005	0.001	<0.001	0.003	0.002	<0.001	0.001
	Max	0.069	0.014	0.038	0.12	0.71	0.027	0.23	0.015	0.003	0.004	0.001	0.001	0.024	0.002	0.005	0.010	0.006	<0.001	0.005
In-dust																				
PM_{10}	Mean	1.30	0.36	0.76	1.78	0.96	1.43	0.39	0.80	0.053	0.006	0.003	0.008	0.43	0.003	0.003	0.009	0.008	0.008	0.006
	St. dev.	0.74	0.33	0.94	2.19	0.55	1.93	0.25	0.96	0.054	0.002	0.001	0.007	0.45	0.001	0.003	0.009	0.003	0.010	0.005
	Min	0.38	0.087	0.086	0.18	0.42	0.053	0.18	0.12	0.012	0.004	0.002	0.002	0.081	0.001	0.001	0.003	0.004	0.002	0.002
	Max	2.5	1.1	3.0	6.9	1.9	5.4	0.78	3.1	0.16	0.007	0.004	0.024	1.5	0.004	0.011	0.032	0.013	0.031	0.014
$PM_{2.5}$	Mean	0.46	0.144	0.41	0.93	0.64	0.28	0.24	0.29	0.028	0.004	0.002	0.006	0.235	0.002	0.002	0.006	0.005	0.005	0.002
	St. dev	0.37	0.118	0.37	0.84	0.21	0.36	0.11	0.29	0.021	0.001	0.001	0.002	0.203	<0.001	0.001	0.001	0.002	0.002	0.001
	Min	0.051	0.011	0.020	0.053	0.32	0.019	0.14	0.014	0.003	0.003	0.002	0.004	0.017	0.001	0.001	0.003	0.003	0.002	0.001
	Max	1.0	0.30	0.93	2.1	0.88	0.95	0.47	0.75	0.053	0.006	0.003	0.007	0.49	0.003	0.004	0.007	0.008	0.008	0.004
PM_1	Mean	0.035	0.011	0.019	0.050	0.45	0.014	0.110	0.009	0.002	0.002	0.001	0.001	0.011	0.001	0.001	0.006	0.004	<0.001	0.002
	St. dev.	0.019	0.003	0.012	0.032	0.18	0.007	0.076	0.005	<0.001	0.001	<0.001	<0.001	0.007	<0.001	0.001	0.003	0.001		0.001
	Min	0.008	0.007	0.007	0.025	0.19	0.006	0.027	0.004	0.002	0.002	0.001	0.001	0.005	0.001	<0.001	0.003	0.002	<0.001	0.001
	Max	0.069	0.014	0.038	0.12	0.71	0.027	0.23	0.015	0.003	0.004	0.001	0.001	0.024	0.002	0.005	0.010	0.006	<0.001	0.005

as evidenced by cluster analysis of particles (see Fig. 2), has not been confirmed.

The relationship between average percentages of elements during the in-dust and non-dust days (Fig. 5) showed that the more typical crustal elements—such as Si, Ti and Al—principally increased during Saharan episodes, especially in $PM_{2.5}$. Fe and Ca also assumed greater importance during in-dust days, but only in the finer fractions.

It should be noted that individual particle analysis by SEM-EDS demonstrated the importance of the [Fe] cluster and Ca component of the [VMC] cluster, especially on non-dust days, strongly suggesting a local origin of these elements. In fact, this contradiction with PIXE analysis results could be explained, at least in part, by a decreased incidence of the [Fe] cluster during in-dust days due to the contribution of large amounts of silicate particles, without implying a similar decrease in the amount of Fe, as also frequently occurs within [Si, Al] cluster particles (Table 1).

Ratios between values of the average concentration of Si and other elements (Fig. 6) take higher values during Saharan events (in-dust days) in all PM fractions, confirming the increased overall importance of this element on those days. The major exception to the trend shown is the Si/Al ratio, which fell from values between 2.5 and 3.2 during non-dust days to lower values, namely between 2.3 and 2.6, during in-dust days. Previous studies have shown a fairly constant Si/Al ratio value during Saharan dust episodes, mostly ranging from 2.13 to 2.18;[25] so, a contribution by another aluminosilicate from a local-regional source that altered this ratio value can be inferred. Therefore, the ratio found during in-dust days could be the result of mixing of two different silicate components: a proximal (local-regional) source that influences the Si/Al ratio values recorded on non-dust days, and a distal source that influences the Si/Al ratio values during Saharan inputs. This could also help explain the variability of the Si/Al ratios highlighted by individual particle analysis (ratios from 1.5 to 3.9).

The March 1st to 4th Saharan dust episode showed a Si/Al ratio value higher than the March 28th to April 1st episode (Table 3). Biggest differences are related to the finer PM fractions.

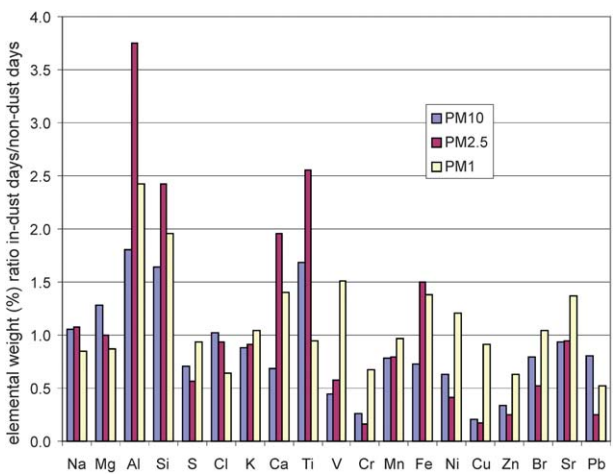

Fig. 5 Weight percent average ratio (in-dust days to non-dust days ratio) for the different fractions of PM.

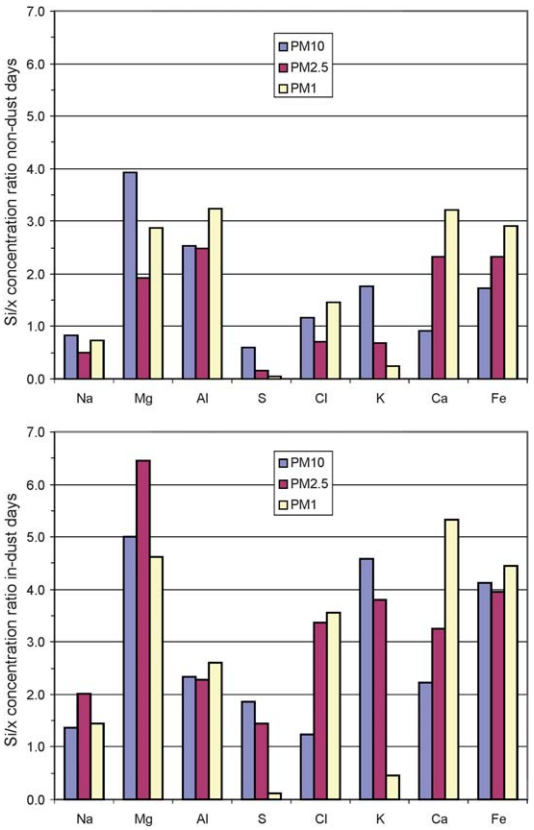

Fig. 6 Average ratios of concentration values (Si to other major elements ratio) for the different fractions of PM, non-dust days (above) and in-dust days (below).

Therefore, according to the back-trajectories and vertical sections of dust concentration (Fig. S1 and S2†), it can be assumed that the first Saharan episode is more influenced by local contribution than the second one. Nevertheless, the difference in Si/Al ratio values may be due to quite separated dust sources.[33]

Other ratios, such as values of the mean concentration of crustal elements *versus* Al, also show differences between non-dust and in-dust days (Fig. S13†). Indeed, a similar decline in ratio values during in-dust days was observed; however, the ratios were still higher than values calculated for Saharan inputs. Only the Fe/Al ratio values during in-dust days (from 0.57 to 0.58) fall within the variability reported for Saharan inputs (values from 0.3 to 5.8), but this variability is the largest among those examined.[25] According to the SEM-EDS analysis results, these ratio values that are higher than those from the literature could point to a mainly local source for elements such as Na, K and Ca, and to a lesser extent Fe.

Table 3 Si/Al ratio at the CR station during the Saharan dust episodes

	Si/Al ratio.		
Saharan dust episode	PM_{10}	$PM_{2.5}$	PM_1
March 1st to 4th	2.38	2.51	3.02
March 28th to April 1st	2.34	2.28	2.51
All days average	2.35	2.30	2.60

4. Conclusion

Analysis of data concerning PM sampled from February 15th to April 15th 2009 in urban and suburban stations in Rome confirmed the influence of episodes of Saharan dust on PM_{10} DLV exceedances in Italy.

Processing of the data acquired by SEM-EDS analysis highlighted the prevalence of complex compositions for individual particles (about 17% were composed of a single element, mainly Fe in PM_{10} and $PM_{2.5}$, and S in PM_1), distinguishing urban from suburban environments and in-dust days from non-dust days. However, the number of "mono-elemental" particles seems inversely correlated to the size of the PM fraction.

Results by cluster analysis showed the following:

- In-dust days were characterised by a higher incidence of the [Si, Al] cluster, due to the influx of Saharan dust in all PM size fractions;

- The [S] cluster, typically connected with anthropogenic pollution, mainly occurred in the PM_1, both on in-dust and non-dust days; however, the widespread distribution of S in the composition of many particles also indicated a trend where secondary sulfate grew on the aerosol particles to form a coating;

- The significance of the [Fe] cluster, highlighted by SEM-EDS analysis of individual particles and especially on non-dust days and in urban areas, declined after the results of the PIXE analysis were examined, emphasising the importance of an integrated approach to the study of PM;

- The [Cl, Na] cluster characterised non-dust days and disappeared during in-dust days;

- The [Si] cluster increased proportionally in PM_1 during in-dust days.

The study has also shown the usefulness of the construction of binary and ternary plots correlating the detected elements, which can aid in the statistical interpretation of data and further clarify relationships between the various contributions and sources.

The [S] cluster particles had dimensions (ECD) that were mostly less than 1 μm, with an aspect ratio even greater than 2 indicating their elongated shape. Moreover, the number of particles by [Si, Al] cluster decreased with decreasing size of particles, showing a wide variation in shape. Finally, the [Cl, Na] cluster particles tended to assume a shape closer to spherical (aspect ratio from 1 to 1.2).

The PIXE analysis supported findings on the particulate components highlighted by SEM-EDS analysis, showing increases in crustal elements in PM during in-dust days (Si, Al and Ti; conversely, less Ca and Fe). Trends for the main element ratios, considering the soils and rock outcrop types near the stations, also suggest a likely contribution by local and/or regional natural sources.

Overall, percentages of contributions attributable to crustal particles were always quite high. For this reason, taking into account the contribution of resuspended particulate could lead to relevant reductions even on the non-dust days, further reducing PM_{10} DLV exceedances.

Acknowledgements

This study was financially supported by the Istituto Superiore per la Protezione e la Ricerca Ambientale (ISPRA) under the ISPRA-CESPRO (Università di Firenze) project "Particulate matter in Italy in the context of the EU air quality legislation review processes," contract 04/3/7359. The authors wish to thank Dr Mario Paolieri and Maurizio Ulivi at Centro Interdipartimentale di Microscopia Elettronica e Microanalisi (MEMA) of the Università di Firenze for providing SEM-EDS instruments and analysis assistance. Many thanks are also due to Dr Francesco Troiano (ARPA Lazio) for necessary support from the regional air quality network. The authors gratefully acknowledge: the NOAA Air Resources Laboratory (ARL) for providing the HYSPLIT transport and dispersion model and READY website (http://www.arl.noaa.gov/ready.html) used in this publication, the NOAA/OAR/ESRL PSD, Boulder, Colorado, USA for providing the NCEP Reanalysis data from http://www.cdc.noaa.gov/ and the Research Centre for Numerical Weather Prediction at Tel-Aviv University (TAU-WeRC) for providing the dust forecast images from http://wind.tau.ac.il/dust8/dust.html.

References

1 A. G. Cook, P. Weinstein and J. A. Centeno, *Biol. Trace Elem. Res.*, 2005, **103**, 1–15; C. M. Bennett, I. G. McKendry, S. Kelly, K. Denike and T. Koch, *Sci. Total Environ.*, 2006, **366**, 918–925; C. Mitsakou, G. Kallos, N. Papantoniou, C. Spyrou, S. Solomos, M. Astitha and C. Housiadas, *Atmos. Chem. Phys.*, 2008, **8**, 7181–7192; E. Ganor, A. Stupp and P. Alpert, *Atmos. Environ.*, 2009, **43**, 5463–5468.

2 P. R. Buseck and M. Pósfai, *Proc. Natl. Acad. Sci. U. S. A.*, 1999, **96**, 3372–3379.

3 M. Escudero, A. Stein, R. R. Draxler, X. Querol, A. Alastuey, S. Castillo and A. Avila, *J. Geophys. Res., [Atmos.]*, 2006, **111**, D06210.

4 M. Escudero, X. Querol, J. Pey, A. Alastuey, N. Pérez, F. Ferreira, S. Alonso, S. Rodríguez and E. Cuevas, *Atmos. Environ.*, 2007, **41**, 5516–5524.

5 J. Nicolás, M. Chiari, J. Crespo, I. Garcia Orellana, F. Lucarelli, S. Nava, C. Pastor and E. Yubero, *Atmos. Environ.*, 2008, **42**, 8872–8882.

6 L. Matassoni, G. Pratesi, D. Centioli, F. Cadoni, P. Malesani, A. M. Caricchia and A. Di Menno di Bucchianico, *J. Environ. Monit.*, 2009, **11**, 1586–1594.

7 X. Querol, J. Pey, M. Pandolfi, A. Alastuey, M. Cusack, N. Pérez, T. Moreno, M. Viana, N. Mihalopoulos, G. Kallos and S. Kleanthous, *Atmos. Environ.*, 2009, **43**, 4266–4277.

8 S. Larssenn, R. Sluyter and C. Helmis, *Criteria for EUROAIRNET. The EEA Air Quality Monitoring and Information Network, Technical Report no. 12*, European Environment Agency, Copenhagen, 1999.

9 L. Matassoni, G. Pratesi, D. Centioli, *Atmos. Environ.*, in press, DOI: 10.1016/j.atmosenv.2010.11.24.

10 Y. Mamane, R. Willis and T. Conner, *Aerosol Sci. Technol.*, 2001, **34**, 97–107.

11 G. S. Casuccio, S. F. Schlaegle, T. L. Lersch, G. P. Huffman, Y. Chen and N. Shah, *Fuel Process. Technol.*, 2004, **85**, 763–779.

12 D. V. Martello, R. R. Anderson, C. M. White, G. S. Casuccio, S. F. Schlaegle and R. J. Lee, *Quantitative Scanning Electron Microscopy Methods to Characterize Ambient Air PM2.5*, Preprints-American Chemical Society, Division of Fuel Chemistry, 2001, vol. 46.

13 P. Kishcha, S. Nickovic, E. Ganor, L. Kordova and P. Alpert, in *Air Pollution Modeling and its Application XIX*, ed. C. Borrego and A. I. Miranda, Springer, New York, 2008, pp. 358–366.

14 M. S. Germani and P. R. Buseck, *Anal. Chem.*, 1991, **63**, 2232–2237; T. L. Conner, G. A. Norris, M. S. Landis and R. W. Williams, *Atmos. Environ.*, 2001, **35**, 3935–3946.

15 J. L. Pouchou and F. Pichoir, in *Electron Probe Quantitation*, ed. K. F. J. Heinrich and D. E. Newbury, Plenum Press, New York, 1991, pp. 31–76; J. L. Pouchou, F. Pichoir and D. Boivin, in *Microbeam*

Analysis-1990, ed. J. R. Michael and P. Ingram, San Francisco Press, San Francisco, 1990, pp. 120–126.
16 P. Del Carmine, F. Lucarelli, P. A. Mandò, G. Moscheni and A. Pecchioli, *Nucl. Instrum. Methods Phys. Res., Sect. B*, 1990, **45**, 341–346; S. Nava, P. Prati, F. Lucarelli, P. A. Mandò and A. Zucchiatti, *Water, Air, Soil Pollut.: Focus*, 2002, **2**, 247–260; M. Chiari, P. Del Carmine, F. Lucarelli, G. Marcazzan, S. Nava, L. Paperetti, P. Prati, G. Valli, R. Vecchi and A. Zucchiatti, *Nucl. Instrum. Methods Phys. Res., Sect. B*, 2004, **219–220**, 166–170; F. Lucarelli, P. A. Mandò, S. Nava, P. Prati and A. Zucchiatti, *J. Air Waste Manage. Assoc.*, 2004, **54**, 1372–1382.
17 M. Chiari, F. Lucarelli, F. Mazzei, S. Nava, L. Paperetti, P. Prati, G. Valli and R. Vecchi, *X-Ray Spectrom.*, 2005, **34**, 323–329.
18 G. Calzolai, M. Chiari, I. García Orellana, F. Lucarelli, A. Migliori, S. Nava and F. Taccetti, *Nucl. Instrum. Methods Phys. Res., Sect. B*, 2006, **249**, 928–931.
19 J. A. Maxwell, W. J. Teesdale and J. L. Campbell, *Nucl. Instrum. Methods Phys. Res., Sect. B*, 1995, **95**, 407–421.
20 T. W. Shattuck, M. S. Germani and P. R. Buseck, in *Environmental Applications of Chemometrics*, ed. J. J. Breen and P. E. Robinson, ACS Symposium Series, American Chemical Society, Washington, DC, 1985, pp. 118–129; T. W. Shattuck, M. S. Germani and P. R. Buseck, *Anal. Chem.*, 1991, **63**, 2646–2656; J. R. Anderson, P. R. Buseck, D. A. Saucy and J. Pacyna, *Atmos. Environ., Part A*, 1992, **26**, 1747–1762; I. Bondarenko, B. Treiger, R. Van Grieken and P. Van Espen, *Spectrochim. Acta, Part B*, 1996, **51**, 441–456.
21 H. Yuan, K. A. Rahn and G. Zhuang, *Atmos. Environ.*, 2004, **38**, 6845–6854.
22 S. C. Alfaro and L. Gomes, *J. Geophys. Res., [Atmos.]*, 2001, **106**, 18075–18084.
23 I. J. Smalley, R. Kumar, K. O'Hara Dhand, I. F. Jefferson and R. D. Evans, *Sediment. Geol.*, 2005, **179**, 321–328.
24 R. Vautard, B. Bessagnet, M. Chin and L. Menut, *Atmos. Environ.*, 2005, **39**, 3291–3303.
25 K. Kandler, N. Benker, U. Bundke, E. Cuevas, M. Ebert, P. Knippertz, S. Rodríguez, L. Schütz and S. Weinbruch, *Atmos. Environ.*, 2007, **41**, 8058–8074.
26 J. R. Anderson, P. R. Buseck and T. L. Patterson, *Atmos. Environ.*, 1996, **30**, 319–338.
27 T. Moreno, W. Gibbons, T. Jones and R. Richards, *Atmos. Environ.*, 2003, **37**, 4265–4276; T. Moreno, T. P. Jones and R. Richards, *Atmos. Environ.*, 2004, **38**, 337–346; J. M. Bernabé, M. I. Carretero and E. Galán, *Atmos. Environ.*, 2005, **39**, 6777–6789; M. Choël, K. Deboudt, P. Flament, L. Aimoz and X. Mériaux, *Atmos. Environ.*, 2007, **41**, 2820–2830; G. Pratesi, M. Zoppi, T. Vaiani and F. Calastrini, *Water, Air, Soil Pollut.*, 2007, **179**, 283–296.
28 R. Salminen, M. J. Batista, M. Bidovec, A. Demetriades, B. De Vivo, W. De Vos, M. Duris, A. Gilucis, V. Gregorauskiene, J. Halamic, P. Heitzmann, A. Lima, G. Jordan, G. Klaver, P. Klein, J. Lis, J. Locutura, K. Marsina, A. Mazreku, P. J. O'Connor, S. A. Olsson, R.-T. Ottesen, V. Petersell, J. A. Plant, S. Reeder, I. Salpeteur, H. Sandström, U. Siewers, A. Steenfelt and T. Tarvainen, *Geochemical Atlas of Europe, Part 1—Background Information, Methodology and Maps*, Geological Survey of Finland, Espoo, 2005.
29 T. Catelani, *MSc thesis*, Università degli Studi di Firenze, 2010.
30 S. Hoornaert, H. Van Malderen and R. Van Grieken, *Environ. Sci. Technol.*, 1996, **30**, 1515–1520.
31 Z. Levin, A. Teller, E. Ganor and Y. Yin, *J. Geophys., Res. [Atmos.]*, 2005, **110**, D20202.
32 G. Coude-Gaussen, P. Rognon, G. Bergametti, L. Gomes, B. Strauss, J. M. Gros and M. N. Le Coustumer, *J. Geophys. Res., [Atmos.]*, 1987, **92**, 9753–9771; A. Chabas and R. A. Lefèvre, *Atmos. Environ.*, 2000, **34**, 225–238; E. Coz, F. J. Gómez-Moreno, M. Pujadas, G. S. Casuccio, T. L. Lersch and B. Artíñano, *Atmos. Environ.*, 2009, **43**, 1850–1863.
33 G. Bergametti, L. Gomes, G. Coude-Gaussen, P. Rognon and M.-N. Le Coustumer, *J. Geophys. Res., [Atmos.]*, 1989, **94**, 14855–14864.

